electronic reprint

Journal of
Applied Crystallography
ISSN 0021-8898
Editor: **Anke R. Kaysser-Pyzalla**

X-ray diffracted intensity for double-reflection channel-cut Ge monochromators at extremely asymmetric diffraction conditions

Claudio Ferrari, Fabrizio Germini, Dusan Korytár, Petr Mikulík and Luca Peverini

J. Appl. Cryst. (2011). **44**, 353–358

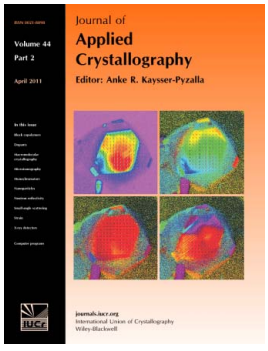

Journal of
Applied Crystallography
ISSN 0021-8898

Received 16 June 2010
Accepted 10 January 2011

X-ray diffracted intensity for double-reflection channel-cut Ge monochromators at extremely asymmetric diffraction conditions

Claudio Ferrari,[a]* Fabrizio Germini,[a] Dusan Korytár,[b] Petr Mikulík[c] and Luca Peverini[d]

[a]CNR IMEM Institute, Viale Usberti 37/A, Parma, 43124, Italy, [b]Institute of Electrical Engineering, SAS, Pieštany, Slovakia, [c]Institute of Condensed Matter Physics, Masaryk University, Brno, Czech Republic, and [d]ESRF, Grenoble, France. Correspondence e-mail: ferrari@imem.cnr.it

The width and integrated intensity of the 220 X-ray double-diffraction profile and the shift of the Bragg condition due to refraction have been measured in a channel-cut Ge crystal in an angular range near the critical angle of total external reflection. The Bragg angle and incidence condition were varied by changing the X-ray energy. In agreement with the extended dynamical theory of X-ray diffraction, the integrated intensity of the double diffraction remained almost constant, even for the grazing-incidence condition very close to the critical angle for total external reflection. A broadening of the diffraction profile not predicted by the extended theory of X-ray diffraction was observed when the Bragg condition was at angles of incidence lower than 0.6°. Plane wave topographs revealed a contrast that could be explained by a slight residual crystal surface undulation of 0.3° due to etching to remove the cutting damage and the increasing effect of refraction at glancing angles close to the critical angle. These findings confirm that highly asymmetric channel-cut Ge crystals can also work as efficient monochromators or image magnifiers at glancing angles close to the critical angle, the main limitation being the crystal surface preparation.

1. Introduction

Double-diffraction channel-cut single crystals are often used as X-ray optical elements for X-ray monochromators as, for instance, in the Bartels (1983) scheme. The advantages of the double diffraction are that the exit beam is in the same direction as the incident beam and that the intensity of the diffracted beam decreases as $\Delta\theta^{-4}$ instead of $\Delta\theta^{-2}$ as in the case of single crystals, $\Delta\theta$ being the angular deviation with respect to the Bragg peak. Symmetric channel-cut Ge crystals are commonly used as monochromators for high-resolution diffractometers.

For channel surfaces parallel to the diffracting planes both diffraction conditions at the two inner surfaces are fulfilled, since the shifts of the Bragg condition due to the refraction effect are equivalent.

The dynamical theory of X-ray diffraction shows that this is verified for any degree of asymmetry for parallel channel surfaces (van der Sluis, 1994), so that there is only a small reduction of the double-diffracted intensity with respect to a single reflection. This is not true in general when the inner surfaces have a different degree of asymmetry because of the different Bragg angle shift at each surface.

On the other hand, channel-cut Ge crystals with different degrees of asymmetry at the two surfaces are interesting as optic elements for X-ray monochromators (Ferrari & Korytar, 2001; Korytár *et al.*, 2005) and for X-ray magnifiers or demagnifiers (Korytár *et al.*, 2003; Köhler & Schäfer, 2002), where the efficiency of the double diffraction is an important parameter.

Hart *et al.* (1995) have observed that, in the special case of 220 Cu $K\alpha$ diffraction in germanium with grazing incidence and symmetric incidence at the first and second surfaces, respectively, the second diffraction condition is almost completely fulfilled because of the almost complete overlap of the two X-ray diffraction profiles, according to the standard dynamical theory.

Moreover, the interest in the grazing-incidence geometry is due to its efficiency in collecting the X-ray intensity emitted by a divergent X-ray source. In fact, according to the dynamical theory the Darwin width of the diffraction profile and the divergence of the exit beam are approximately linearly dependent on the factors $(|b|)^{1/2}$ and $(|b|^{-1})^{1/2}$, respectively, where $b = -\sin(\theta_B - \varphi)/\sin(\varphi + \theta_B)$ is the asymmetry factor, with φ the asymmetry angle, negative for grazing incidence, and θ_B the Bragg angle of the diffraction. On the basis of these results, grazing-incidence asymmetric crystals have been proposed as efficient collimating X-ray optic elements (see, for instance, Renninger, 1966).

More recently Servidori (2002) has proposed a high-efficiency mixed-asymmetry channel-cut Ge monochromator with

a higher diffracted intensity and a lower beam divergence with respect to a conventional Bartels-type monochromator based on symmetric channel surfaces. In the Servidori monochromator a grazing angle of 1° for the first surface was considered, at nearly 0.6° from the critical angle for the Cu $K\alpha$ wavelength in germanium.

To date, no experimental evidence of the advantages of this monochromator has been reported; moreover, in view of using mixed-asymmetry channel-cut crystals as X-ray optic elements, it is interesting to investigate their behaviour at angles of incidence close to the critical angle for total external reflection, when the standard dynamical theory is no longer applicable.

2. Experimental

2.1. Crystal preparation

The channel-cut crystal was obtained from a monolithic piece of germanium using a diamond saw. The inner cuts were performed to obtain asymmetry angles of 22.05 and 9° for the first and second surfaces, respectively, for the 220 Cu $K\alpha_1$ diffraction (θ_B = 22.65°) corresponding to $b_1 = -67$ and $b_2 = -0.41$, respectively.

The crystal was then lapped with coarse and fine lapping powders and later polished with fine diamond paste. To remove the remnants of mechanical damage, the crystal was manually chemo-mechanically polished with a wheel and a vibrating device, and finally chemically polished in a modified HF, HNO_3, CH_3COOH solution. This is a standard procedure for producing symmetric and asymmetric channel-cut Ge crystals employed as monochromators in high-resolution diffractometers. At the end of this process all the internal and external surfaces showed a mirror-like appearance to the naked eye.

2.2. Diffraction measurements

In order to check the accuracy of the cutting process the asymmetry angle of the first surface of the channel-cut Ge crystal was verified. By using an open-window detector it was possible to measure in the same scan the diffraction and the reflectivity profiles as a function of the glancing angle, using the reflectivity profile as a reference and avoiding the error arising from the zero-angle offset. The position of the critical angle for total external reflection was assumed at 50% of the maximum intensity of the reflectivity profile on the high-angle side of the peak. The decrease in the reflected intensity at the low-angle side of the peak is an instrumental effect due to the finite size of the sample.

The refraction-induced angular shift of the Bragg peak as a function of angle of incidence was calculated following James (1963) or Rustichelli (1975):

$$\Delta\theta = \frac{|\Phi_0|}{2\sin 2\theta_B}\left(1 + \left|\frac{\gamma_H}{\gamma_0}\right|\right). \quad (1)$$

Here γ_0 and γ_H represent the direction cosines of the incident and diffracted beam, respectively, with respect to the surface normal directed into the crystal:

$$\gamma_0 = \sin(\theta_B - \alpha) \quad \text{and} \quad \gamma_H = -\sin(\theta_B + \alpha). \quad (2)$$

θ_B and α are the Bragg angle and the asymmetry angle, respectively, Φ_0 and Φ_H represent the Fourier component of indexes 0 and H, respectively, of 4π times the polarizability.

From the calculated value of the refraction-induced angular shift (+0.07°) and the measured 0.37° angular separation between the critical angle (θ_C = 0.31° for Cu $K\alpha$ in germanium) and the 220 Cu $K\alpha_1$ peak, we evaluated an asymmetry angle of 22.04 (5)° for the first crystal surface with respect to the (110) planes, in good agreement with the nominal value of 22.05°.

The channel-cut crystal was tested using a standard fine-focus Cu X-ray tube and line source. In Fig. 1 we compare the 220 diffraction profiles of a symmetric channel-cut 220 Ge crystal and of our crystal using the grazing incidence as the first diffraction. In both measurements we used the same X-ray generator power (10 kV, 10 mA), the same source–detector distance and the same 2 mm slit in front of the detector. Because of the large divergence of the incident

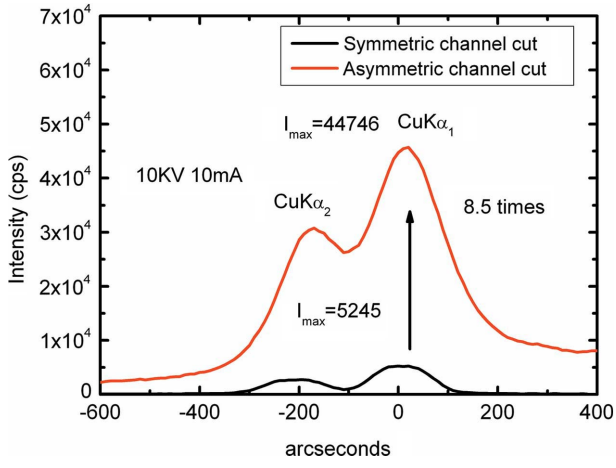

Figure 1
Comparison between Cu $K\alpha$ diffraction profiles obtained from a symmetric and the present mixed-geometry Ge 220 channel-cut crystals taken in the same experimental conditions and using a fine-focus X-ray tube.

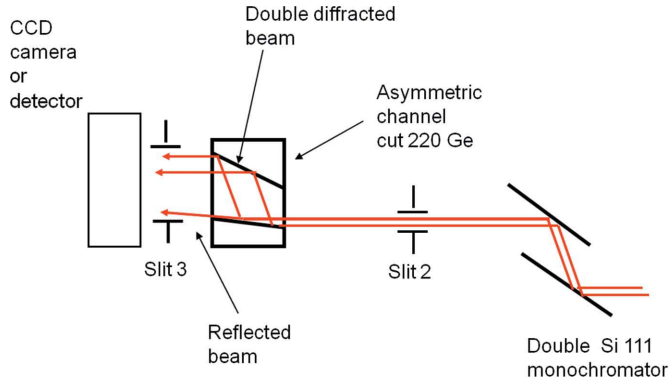

Figure 2
Scheme of the experimental setting used at the synchrotron for the measurements. By adjusting slit 3 it was possible to measure the reflected and the diffracted beams at the same time.

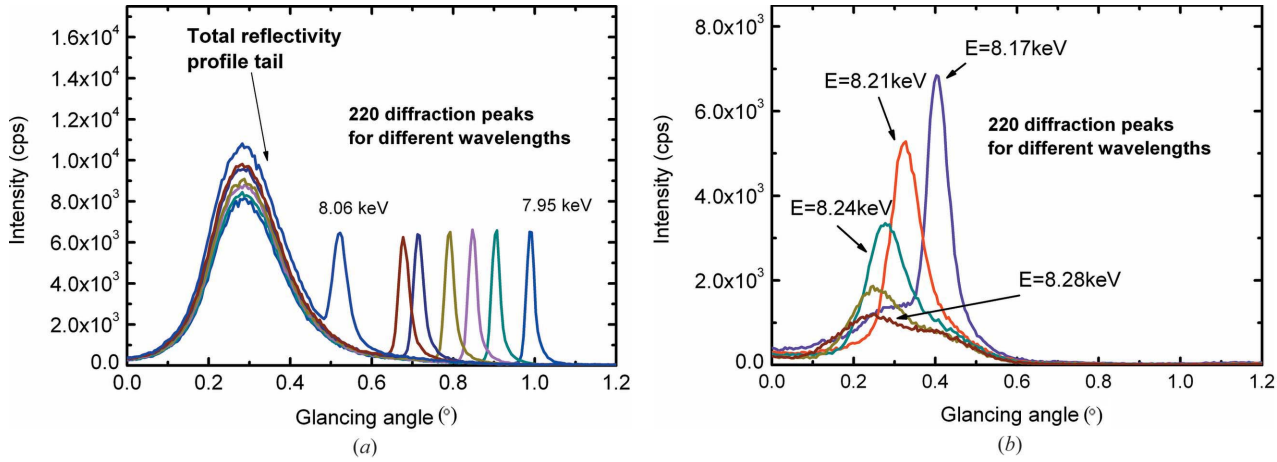

Figure 3
(*a*) Combined double-diffracted and reflected profiles at different energies. According to the peak position from higher to lower angles the X-ray beam energies are 7.95, 7.98, 8.0, 8.02, 8.04, 8.047 and 8.06 keV. (*b*) Double-diffracted X-ray profiles at 8.17, 8.21, 8.24, 8.26 and 8.28 keV.

beam, the peak intensity is proportional to the integrated intensity of the theoretical profiles.

The ratio between the Cu $K\alpha_1$ peaks in the two profiles is almost coincident with the ratio of the 220 Ge theoretical integrated intensities of the symmetric ($b = -1$) and asymmetric ($b = -67$) single-crystal diffraction profiles calculated using the dynamical theory. This confirms that the second diffraction does not reduce significantly the final intensity (Hart *et al.*, 1995) with respect to a single grazing-incidence diffraction and that the grazing–nearly symmetric mixed geometry enhances the collection efficiency of the monochromator (Servidori, 2002).

To study the dependence of diffracted intensity profiles as a function of the glancing angle $\theta_B + \varphi$ (that is, the angle between the incident beam at the Bragg condition and the crystal surface for the grazing-incidence geometry), we have followed the method of Kimura *et al.* (1994) in which the Bragg angle was varied by changing the beam energy using an Si 111 double monochromator out of the synchrotron spectrum. The experimental setting used at the synchrotron is reported in Fig. 2. The Si 111 monochromator was used to select a beam energy in the range 7.8–8.28 keV with an energy resolution of $\Delta E/E = 10^{-3}$. A slit of 1 mm in width and perpendicular to the scattering plane was set in front of the channel-cut sample. A slit between the sample and the detector permitted us to choose between two measuring modes: the diffracted beam only or the diffracted and the reflected beams at the same time, the latter used as a reference.

A set of the double-diffracted profiles are reported in Figs. 3(*a*) and 3(*b*). In Fig. 3(*a*) the reflectivity profiles used as a reference are also reported. In Fig. 4 the integrated intensity of the double-diffraction peak, that is the area of the Bragg peak, is reported as a function of the grazing angle of the Bragg condition.

From Figs. 3 and 4 we notice that (*a*) the integrated intensity of the double-diffracted peak increases slowly when the Bragg peak approaches the critical angle; (*b*) the Bragg peak shifts to lower angles by increasing the beam energy – this shift is due to the decrease of the Bragg angle and to the increase of the refraction-induced Bragg angle shift; (*c*) the FWHM of the diffraction profile increases as the glancing angles decrease; and (*d*) some diffracted intensity is still present even for glancing angles apparently lower than the critical angle.

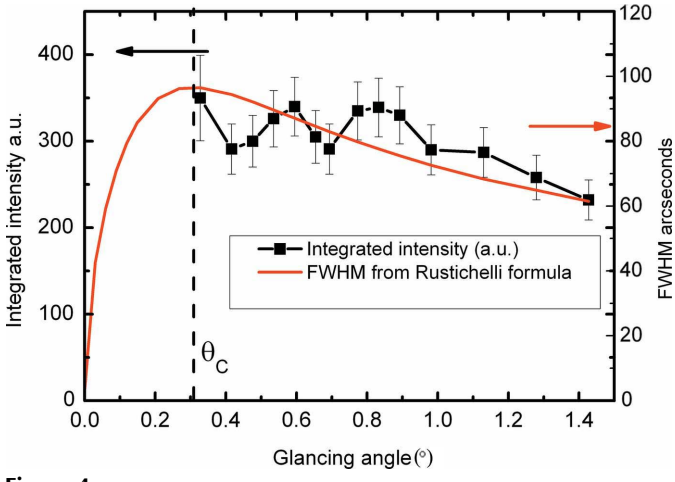

Figure 4
Experimental integrated intensities of the curves of Fig. 3 and the theoretical FWHM calculated from equation (4) as a function of the glancing angle.

3. Discussion

The exact formulation of the extended dynamical theory valid when the incidence angle approaches the critical angle for total external reflection is quite complicated so the diffraction profiles are calculated using numerical methods. In the Bragg case and for low incidence angles, the simplified approach of Rustichelli (1975) takes into account the correct shape for the asymptotic form of the dispersion surface and has the advantage of simple analytical expressions even if neglecting the X-ray absorption in the crystal. Moreover, as pointed out by Afanasev (1992), such an approach is quite accurate in predicting the refraction-induced Bragg shift and the angular

width of the Bragg peak (Darwin width), which is proportional to the integrated intensity.

The Darwin width $\Delta\theta_B$ of the diffraction peak as a function of the glancing angle $(\theta_B - \alpha)$ is given by

$$\Delta\theta_B = \frac{-\gamma_0}{\left[\gamma_0^2 + \frac{\gamma_0|\Phi_0|}{\sin 2\theta_B}\left(1 - \frac{\gamma_H}{\gamma_0}\right)(1-\gamma_0^2)^{1/2}\right]^{1/2}} \times \frac{2|\Phi_H|}{\sin 2\theta_B}\left(\frac{|\gamma_H|}{\gamma_0}\right)^{1/2} \quad (3)$$

and the formula for the refraction-induced Bragg angle shift $\Delta\theta$ is

$$\Delta\theta = \frac{-\gamma_0 + \left[\gamma_0^2 + \frac{\gamma_0|\Phi_0|}{\sin 2\theta_B}\left(1 - \frac{\gamma_H}{\gamma_0}\right)(1-\gamma_0^2)^{1/2}\right]^{1/2}}{(1-\gamma_0^2)^{1/2}}. \quad (4)$$

With respect to the standard dynamical theory, this formula predicts a maximum of the Bragg angle shift when the incidence angle at the Bragg condition approaches the critical angle for total external reflection.

For the sake of simplicity, in the analysis of the experimental results we have assumed a constant 220 structure factor in the energy range between 7.8 and 8.28 keV. This is justified by the limited 5% variation of the wavelength in the interval considered. Moreover, we have neglected the instrumental broadening due to the non-perfect monochromaticity and divergence of the beam from the 111 Si monochromator. These two terms induce a few arcseconds' broadening for Bragg peak widths of the same order but this becomes negligible when the FWHM of the double-diffracted peak is larger than a few tens of arcseconds.

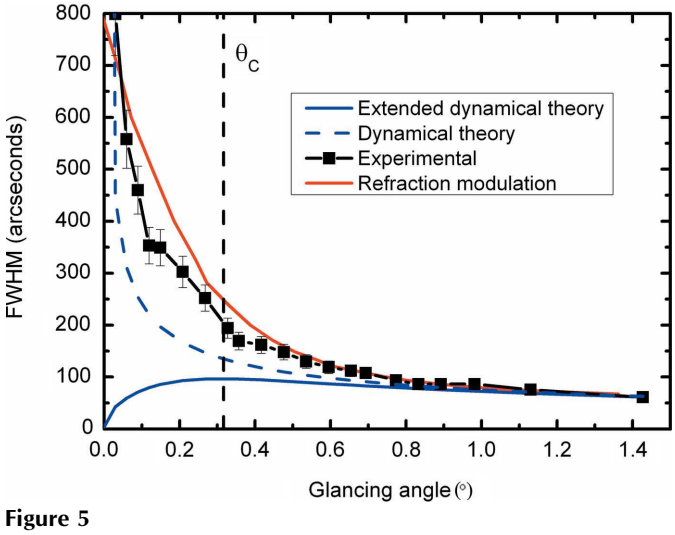

Figure 5
Comparison between the experimental FWHM (square symbols) of the curves of Fig. 3 and the values of the Darwin width as a function of the glancing angle calculated according to the standard and extended dynamical theory. An error bar of 10% has been considered. The refraction modulation curve is calculated by adding the effect of a Bragg shift spread coming from a surface undulation of 0.3° to the Darwin width as given by the extended dynamical theory.

In Fig. 4 the integrated intensity of the double-diffracted peak and the FWHM of the single diffraction peak for the first surface as calculated from equation (3) are reported as a function of the glancing angle. The integrated intensity is an indication of the efficiency of the monochromator in collecting the X-ray beams emerging from a divergent X-ray source, such as for instance a laboratory X-ray tube. We observe in Fig. 4 that, within the statistical error, the integrated intensity has the same dependence as the theoretical FWHM for a single asymmetric diffraction and that there is no intensity decrease when the glancing angle approaches the critical angle θ_C, as in the case of a single Ge 220 diffraction (Kishino & Kohra, 1971; Härtwig, 1981). This demonstrates that, even in the case of very low values of the glancing angle, the refraction effect does not introduce an angular mismatch between X-ray diffraction profiles of the first and second surfaces, as observed for larger angles of incidence (Hart *et al.*, 1995; Servidori, 2002).

This is not true in general for other materials or reflections. For instance, Kimura *et al.* (1994) and Brummer *et al.* (1976) reported a decrease of the peak width and intensity in silicon for the 113 or 555 single reflections for the grazing-incidence geometry near the critical angle.

Fig. 5 shows a comparison between experimental FWHMs of the double-reflection profile and the width predicted by the standard and by the extended dynamical theory for single diffraction as a function of the grazing-incidence angle. For grazing angles down to 1.0°, corresponding to the asymmetry angle considered by Servidori (2002), the dynamical and the extended dynamical theory are comparable. For lower glancing angles the FWHM predicted by the extended dynamical theory reaches a maximum at the critical angle $\theta_C = 0.31°$. A large discrepancy between experimental and theoretical data is apparent.

In Fig. 6 the refraction-induced Bragg angle shift calculated from equation (4) is compared with the experimental data.

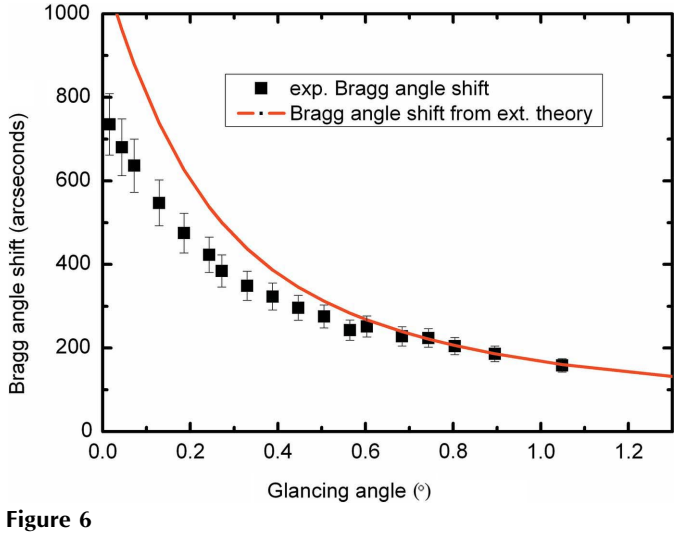

Figure 6
Comparison between experimental (square symbols) and calculated values (line) of the Bragg angle shift as predicted by the extended dynamical theory.

The observed refraction-induced Bragg shift increases less than predicted by the extended dynamical theory when approaching the critical angle.

To understand the origin of such discrepancies a topography of the intensity distribution of the double-diffracted beam has been performed using the CCD camera at the ID19 ESRF beamline for two different positions of the incident beam at a beam energy of 8.13 keV. The working points for the two topographs have been chosen at opposite sides of the 8.13 keV 220 diffraction peak of Fig. 3. For an X-ray beam energy of 8.13 keV, the Bragg peak is approximately 0.12° from the critical angle. Under these conditions the contrast is very sensitive to small, local deviations of the incidence angle. The topographs of Fig. 7 show a striation contrast perpendicular to the projections of the incident and diffracted beams on the plane of the figure. It is noteworthy that the contrast reverses at the two opposite flanks of the Bragg peak. Since every part of the crystal can reach the diffraction condition by slightly rotating the crystal, this contrast cannot be explained by a simple shadowing effect induced by the imperfect surface planarity.

It is worth noting that the deep etching (several tens of μm) after the cutting procedure can exclude the possibility of residual surface damage explaining the observed contrast of Fig. 7 or the peak broadening of Fig. 5. We can also rule out scattering effects related to short-scale surface roughness and to the coherence length of the synchrotron radiation used, which is of the order of 100 μm for the ESRF ID19 and less than that at the ANKA PDIFF (Karlsruhe Institute of Technology) beamlines, since this effect would be visible even at higher angles of incidence.

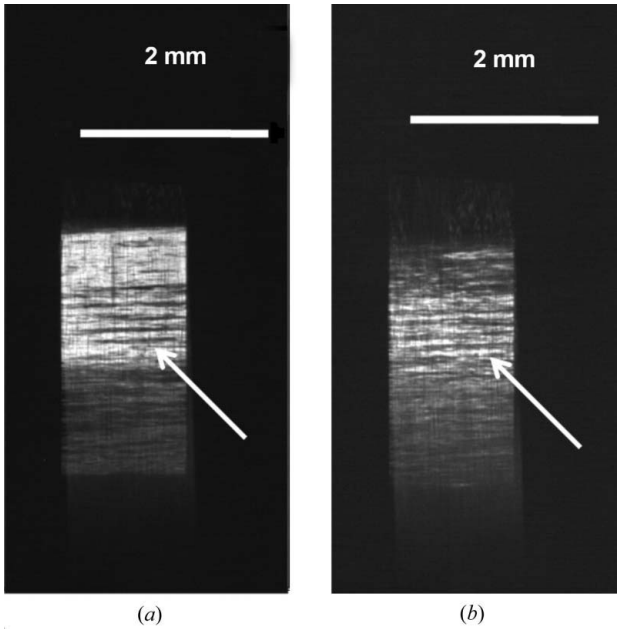

Figure 7
X-ray plane wave topographs of the diffracted beam taken at the two sides of the 220 double-diffracted peak for a beam energy of 8.13 keV at approximately 70% of the peak intensity. (*a*) and (*b*) correspond to the higher- and the lower-angle side, respectively. The arrows indicate the same zone of the crystal with opposite contrast.

We propose that the observed contrast is due to the residual surface undulation (long-scale roughness) induced by the etching of the crystal used to remove the saw surface damage.

As visible from Fig. 6 the refraction-induced Bragg shift increases rapidly when the glancing angle approaches the critical angle so that a local change of surface inclination can induce a contrast visible in X-ray topography. This effect can, in principle, be responsible for the topographic contrast seen by Kimura *et al.* (1994) in a silicon sample at very low glancing angles.

To verify this point, an X-ray reflectivity measurement on the inner surface of the channel-cut Ge crystal has been performed using a high-resolution Expert-Pro Philips diffractometer. The collimating optic consists of a four-reflection Bartels monochromator. Several ω–2θ scans with different ω offset angles have been performed and are reported in Fig. 8. The region of specular reflectivity visible as the most intense spot in the centre of the map appears broadened along the ω direction. From the transverse ω scan performed at $2\theta = 0.5°$ shown in the inset of Fig. 8 we estimate a 0.3° broadening which can be associated with a long-range surface undulation. Such a broadening was not seen in equivalent measurements performed on silicon or germanium wafers, where the planarity of the crystal surface is in general limited to a few nm in height.

The red curve in Fig. 5 was calculated by adding the Bragg shift spread $\Delta\theta_S$ given by a surface undulation of 0.3° to the Darwin width as calculated by equation (1) using the approximation

$$\mathrm{FWHM}_{\mathrm{Tot}} = (\Delta\theta_C^2 + \Delta\theta_S^2)^{1/2}, \qquad (5)$$

strictly valid for Gaussian curves. Equation (5) is able to explain, at least qualitatively, the observed deviation.

The presence of surface undulation can also explain the observed diffracted intensity even below the critical angle θ_C,

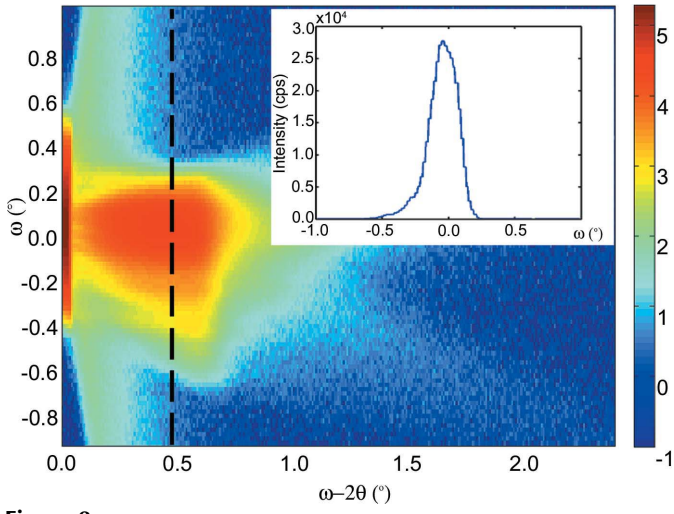

Figure 8
Two-dimensional scan in the space ω, ω–2θ. The vertical section of the figure in the region of specular reflection and reported in the inset corresponds to a transverse scan for a fixed $2\theta = 0.5°$ position of the detector. The diffuse scattering at low ω–2θ angles corresponds to the Yoneda (1963) wings.

and the discrepancy between theoretical and experimental values of the refraction-induced Bragg angle shift of Fig. 6, if we consider that the parts of the crystal corresponding to lower values of angle of incidence ($<0.3^\circ$) are shadowed by undulation at very low angles of incidence.

4. Conclusions

We have investigated the width and position of the double-diffraction peak in an asymmetrical channel-cut Ge 220 crystal in an angular range very close to the critical angle of total external reflection by varying the X-ray beam wavelength. We have found that the intensity of the double-diffracted beam was nearly equivalent to the intensity of the single grazing-incidence diffracted beam even for Bragg peak positions very close ($<0.1^\circ$) to the critical angle for total external reflection. We then concluded that for this 220 Ge-based mixed-asymmetry monochromator the refraction effect does not modify significantly the coincidence of Bragg conditions at the first and second surfaces.

An unexpected broadening of the diffraction profile observed for Bragg peaks set at angles of incidence close to the critical angle can be explained by a surface undulation of the order of $\pm 0.3^\circ$ due to the standard preparation of the crystal inner surfaces, performed by diamond saw and chemical etching.

Plane wave topography revealed a contrast resulting from the combined effects of the surface undulation and the large shift of Bragg angle position due to the refractive index at glancing angles very close to the critical angle. We determined that this large surface undulation produces a negligible effect on the double-diffracted peak width and intensity for glancing angles larger than approximately 0.6°.

These findings confirm that highly asymmetric channel-cut Ge crystals prepared by diamond saw and chemical etching may perform as perfect crystals for glancing angles down to approximately 0.6° but, in principle, channel-cut crystals working at very low glancing angles can be used as monochromators or image magnifiers with proper surface preparation.

This work has been supported by the bilateral project 'Semiconducting crystals for X-ray optics, gamma-ray detectors and solar cells' between IMEM-CNR and IEE SAS, by the Slovak Research and Development Agency under contract No. APVV-0459-06, and by the COST MP0601 Action. PM acknowledges support (grant No. MSM 0021622410) from the Ministry of Education of the Czech Republic. The synchrotron measurements were supported by the ESRF in Grenoble and ANKA in Karlsruhe, and performed at the ID19 and PDIFF beamlines, respectively.

References

Afanasev, A. M. (1992). *Crystallogr. Rev.* **3**, 157–230.
Bartels, W. J. (1983). *J. Vac. Sci. Technol. B*, **2**, 338–345.
Brummer, O., Hoche, H. R. & Nieber, J. (1976). *Phys. Status Solidi A*, **37**, 529–532.
Ferrari, C. & Korytar, D. (2001). *J. Appl. Cryst.* **34**, 608–612.
Hart, M., Koga, T. & Takano, Y. (1995). *J. Appl. Cryst.* **28**, 568–570.
Härtwig, J. (1981). *Acta Cryst.* A**37**, 802–804.
James, R. W. (1963). *Solid State Phys.* **15**, 53–220.
Kimura, S., Harada, J. & Ishikawa, T. (1994). *Acta Cryst.* A**50**, 337–342.
Kishino, S. & Kohra, K. (1971). *Jpn. J. Appl. Phys.* **10**, 551–567.
Köhler, R. & Schäfer, P. (2002). *Cryst. Res. Technol.* **37**, 734–746.
Korytár, D., Baumbach, T., Ferrari, C., Helfen, L., Verdi, N., Mikulík, P., Kubena, A. & Vagovic, P. (2005). *J. Phys. D Appl. Phys.* **38**, A208–A212.
Korytár, D., Mikulík, P., Ferrari, C., Hrdý, J., Baumbach, T., Freund, A. & Kuběna, A. (2003). *J. Phys. D Appl. Phys.* **36**, A65–A68.
Renninger, M. (1966). *Adv. X-ray Anal.* **10**, 32–41.
Rustichelli, F. (1975). *Philos. Mag.* **31**, 1–12.
Servidori, M. (2002). *J. Appl. Cryst.* **35**, 41–48.
Sluis, P. van der (1994). *J. Appl. Cryst.* **27**, 50–55.
Yoneda, Y. (1963). *Phys. Rev.* **131**, 2010–2013.